We are IntechOpen,
the world's leading publisher of
Open Access books
Built by scientists, for scientists

6,900
Open access books available

185,000
International authors and editors

200M
Downloads

Our authors are among the

154
Countries delivered to

TOP 1%
most cited scientists

12.2%
Contributors from top 500 universities

BOOK CITATION INDEX
CLARIVATE ANALYTICS
INDEXED

WEB OF SCIENCE™

Selection of our books indexed in the Book Citation Index
in Web of Science™ Core Collection (BKCI)

Interested in publishing with us?
Contact book.department@intechopen.com

Piezoelectric Properties and Microstructure of (K,Na)NbO$_3$–KTiNbO$_5$ Composite Lead-Free Piezoelectric Ceramic

Kazushige Ohbayashi

Abstract

We developed a (K,Na)NbO$_3$-based lead-free piezoelectric ceramic with a KTiNbO$_5$ system, $(K_{1-x}Na_x)_{0.86}Ca_{0.04}Li_{0.02}Nb_{0.85}O_{3-\delta}$–KTiNbO$_5$–BaZrO$_3$–Co$_3O_4$–Fe$_2O_3$–ZnO (KNN–NTK composite). This KNN–NTK composite exhibits a very dense microstructure, and k_p = 0.52, $\varepsilon_{33}^T/\varepsilon_0$ = 1600, and d_{33} = 252 pC/N. We found that a portion of the KTiNbO$_5$ converted into K$_2$(Ti,Nb,Co,Zn)$_6$O$_{13}$ and/or CoZnTiO$_4$. We were able to reproducibly prepare granulated powder of KNN–NTK in batches of 100 kg using a spray-dryer. In addition, we performed a detailed investigation of the microstructure of KNN–NTK composite. The results show that a tetragonal and an orthorhombic phase coexist in a main KNN phase over a wide range of $0.56 \leq x \leq 0.75$. The granular nanodomains of the orthorhombic phase dispersed within the tetragonal matrix in the KNN phase. A maximum value of k_p = 0.56 occurred for x = 0.56. The Na fraction x corresponding to maximum k_p was also the minimum x required to generate the orthorhombic phase. We conclude that the KNN–NTK composite exhibits excellent piezoelectric properties because of the two-phase coexisting state. This gentle phase transition of KNN–NTK composite seems to be a relaxor, but the diffuseness degree γ = 1.07 suggests otherwise.

Keywords: (K,Na)NbO$_3$, lead-free, microstructure, two-phase coexisting, coupling coefficient

1. Introduction

1.1. Improvement of microstructure of (K,Na)NbO$_3$-based lead-free piezoelectric ceramic with KTiNbO$_5$ phase

Recently, the development of lead-free piezoelectric ceramics as substitutes for lead zirconate titanate (PZT) has become an important objective. Alkaline niobate ceramics (K,Na)NbO$_3$ exhibit particularly high piezoelectric characteristics and a relatively high Curie temperature (*Tc*). However, the crystalline particles of these ceramics spontaneously form dice-like particles, which tend to generate voids between particles. The presence of an excessive number of voids in a sintered ceramic decreases its chemical stability and mechanical strength and facilitates dielectric breakdown during polarization because the electric field concentrates at the voids. Our research shows that these voids may degrade the piezoelectric properties of these materials. If this problem can be resolved, alkaline niobate ceramics could see use in practical applications; for example, in ultrasonic motors [1, 2], actuators [3], inkjet heads [4, 5], and transducers [6].

The preparation of alkaline niobate ceramics with high piezoelectric properties has been reported, the hot-press sintering method which decreases the crystal grain size, increases the density of the ceramics from 4.25 to 4.46 g/cm^3, and doubles the piezoelectric constant d_{33} from 80 to 160 pC/N [7]. For KNN prepared using the reactive-templated grain growth method, Saito et al. [8] reported a high piezoelectric constant of d_{33} = 416 pC/N, which is equivalent to that of PZT.
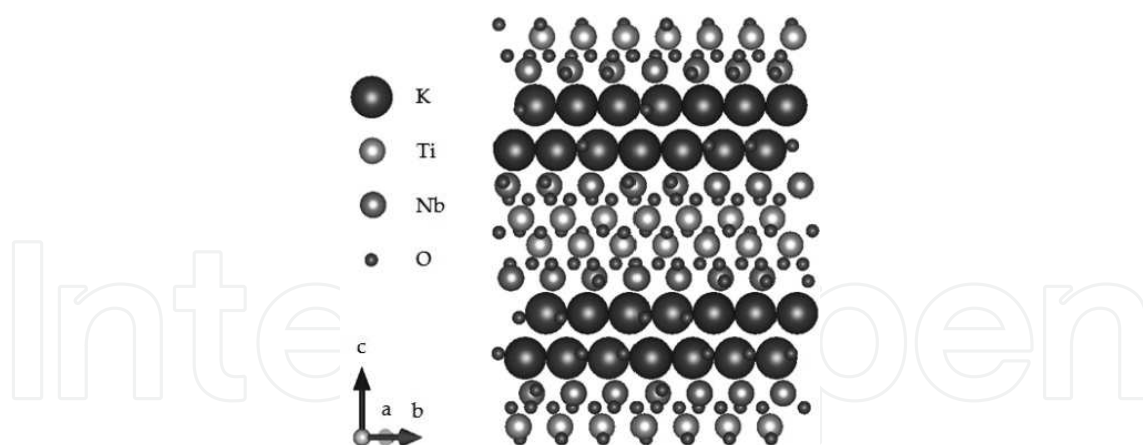

Figure 1. Crystal structure of KTiNbO$_5$ has a layered structure and is not piezoelectric material.

Although KNN has been reported to exhibit attractive piezoelectric characteristics, problems such as stability and productivity remain. Consequently, alkaline niobate ceramics are still under development. To fill these voids, we focus on combining KNN with a dielectric material. An example of such an approach was reported [9] that a glass phase (e.g., K$_3$Nb$_3$O$_6$Si$_2$O$_7$) was added to KNN to improve the insulating characteristics of KNN by decreasing the particle diameter and the number of voids.

In our present study [10, 11], after due consideration of the dielectric constant, we combine KNN with the KTiNbO$_5$ (NTK) phase, which has a layered structure as shown in **Figure 1** and is not piezoelectric material. With this approach, we prepared and densified a KNN–NTK composite ceramic that exhibits enhanced piezoelectric properties; notably, a planar-mode electromechanical coupling coefficient $k_p = 0.52$, which is close to the highest value previously reported for KNN-based composite lead-free piezoelectric ceramics [8, 12–15].

1.2. Tetragonal and orthorhombic two-phase coexisting state in KNN–NTK composite lead-free piezoelectric ceramic

As described above, the KNN–NTK composite lead-free piezoelectric ceramic exhibits excellent piezoelectric properties. However, the crystal structure of the main phase of this KNN composite system has yet to be fully determined. Thus, the crystal structure must be elucidated before the piezoelectric properties of this material can be exploited. The crystal structure of KNN-based piezoelectric ceramics has been investigated by many groups [16–19]. For example, Ahtee and Glazer [20], Ahtee and Hewat [21], and Baker et al. [22, 23] proposed phase diagrams for undoped KNN for various values of Na fraction x, where $x =$ Na/(K + Na). With increasing temperature and for $x \leq 0.5$, the crystal system of an undoped KNN ceramic with a perovskite-type structure is suggested to change from orthorhombic to tetragonal and then to cubic.

Many reports exist stating that the crystal system of KNN can be controlled using additives. The orthorhombic–tetragonal polymorphic phase transition temperature may even be lowered below room temperature [24, 25]. Guo et al. [25] reported that the main phase of LiNbO$_3$-doped KNN ceramic is a tetragonal system at room temperature. Rubio-Marcos et al. [26, 27] reported how KNN is affected by doping with the fourth-period transition metal oxides, MO (M = Ni, Cu, Co, and Mn). Based on powder X-ray diffraction (XRD) studies, they concluded that the $P4mm$ tetragonal structure of KNN is stabilized in MO-doped KNN ceramics at room temperature. They also suggest that the tetragonality aspect ratio c/a correlates with the piezoelectric properties of the doped KNN system.

Optimizing the morphotropic phase boundary (MPB) composition is widely thought to improve the properties of piezoelectric materials. Dai et al. [28] reported the dependence of the crystal system and piezoelectric properties of an undoped K$_{1-x}$Na$_x$NbO$_3$ system in the composition range for $0.48 \leq x \leq 0.54$. They assumed that the MPB composition of undoped KNN lies within this range of Na fraction and suggested that the MPB exists in the range $x =$ 0.520–0.525 at room temperature, which separates monoclinic and orthorhombic phases. The maximum piezoelectric constant $d_{33} = 160$ pC/N occurs at $x = 0.52$. Recently, Karaki et al. reported that the slope of the MPB in the BaZrO$_3$–KNN binary system is adjustable. Upon increasing the (Bi,Na)TiO$_3$ content, the slope of the tetragonal–rhombohedral MPB slope of BaZrO$_3$–KNN changes from negative to positive [29].

In this work, we investigate the crystal structure, texture, and piezoelectric properties of a series of KNN-based composite systems (K$_{1-x}$Na$_x$)CaLiNb–NbTiK–BaZr–CoFeZn, using synchrotron powder XRD, high-resolution transmission electron microscopy (HR-TEM), selected-area electron diffraction (SAD), while varying the K/Na ratio over the range $0.33 \leq x$

≤ 0.75. The results clarify that the granular nanodomains of the orthorhombic phase dispersed within the tetragonal matrix are in a KNN phase. Furthermore, we identify a relationship between the piezoelectric properties and the two-phase coexisting state, which reads to the conclusion that the KNN–NTK composite lead-free piezoelectric ceramic exhibits excellent piezoelectric properties because of the two-phase coexisting state.

2. Experimental method

The samples were prepared by a conventional solid-state reaction method. The raw materials were powders of K_2CO_3, Na_2CO_3, Li_2CO_3, Nb_2O_5, $CaCO_3$, TiO_2, $BaCO_3$, ZrO_2, Co_3O_4, Fe_2O_3, and ZnO with a purity of more than 99%. Here, $K_{1-x}Na_xN$, NTK, and BZ refer to $(K_{1-x}Na_x)_{0.86}Ca_{0.04}Li_{0.02}Nb_{0.85}O_{3-\delta}$, $K_{0.85}Ti_{0.85}Nb_{1.15}O_5$, and $BaZrO_3$, respectively. At the outset, hygroscopic powders of K_2CO_3, Na_2CO_3, and Li_2CO_3 were dried in an oven at 150°C for 2 h to ensure accurate weighing. The masses of $K_{1-x}Na_xN$, NTK, and BZ corresponding to their respective composition formulas were weighted out, after which the materials, were calcined at 930°C in air for 4 h.

The calcined powders were again weighed assuming the chemical formula $0.92K_{1-x}Na_xN$–$0.047NTK$–$0.023BZ$–$0.0017Co_3O_4$–$0.002Fe_2O_3$–$0.005ZnO$ (x = 0.51) and $0.910K_{1-x}Na_xN$–$0.042NTK$–$0.036BZ$–$0.0016Co_3O_4$–$0.0025Fe_2O_3$–$0.0069ZnO$ (x = 0.33, 0.42, 0.50, 0.56, 0.58, 0.61, 0.67, 0.71, and 0.75).

The weighed powders were mixed with a ball mill for 15 h and then re-calcined at 930°C in air for 4 h. The dispersant and binder were added to the calcined powder, and the mixture was ball-milled for 15 h. The slurry was filtered through a 25 μm mesh sieve and dried, and the dried powder was classified with a 250 μm mesh sieve. The classified powders were pressed into discs under a uniaxial pressure of 200 kg/cm². The samples were sintered in air at 1150°C for 4 h, following which they were polished and silver electrodes were painted onto both surfaces of the samples. The samples used for electrical properties measurements were 35 mm in diameter and 2 mm in thick for x = 0.51, and 15 mm in diameter and 1 mm in thick for x = 0.33, 0.42, 0.50, 0.56, 0.58, 0.61, 0.67, 0.71, and 0.75 for the planar and thickness vibration modes. For the transverse-, longitudinal-, and shear-vibration mode, the samples dimensions were, 23 × 3 × 0.15 mm, 2.2 mm in diameter and 8 mm in thick, and 7 × 2 × 0.2 mm, respectively. The samples were polarized for 30 min in silicone oil under an electric field of 6 kV/mm at 80°C.

The piezoelectric properties of 1-day-old samples were measured using the resonance–antiresonance method with Hewlett-Packard 4194A impedance analyzer. The mechanical characteristics of 3 × 4 × 40 mm were evaluated according to the Japan Industrial Standard R 1607.

XRD samples were prepared by grinding particles with a 10 μm initial diameter in a Si_3N_4 mortar. The resulting fine powder was sealed in a 0.3 mm diameter Lindemann glass capillary. XRD measurements were done at the BL19B2 beam line of SPring-8 synchrotron, which is equipped with a Debye–Scherrer camera. The incident X-ray wavelength was estimated to be 0.69948 Å by calibration with a standard CeO_2 specimen. The crystal structure was analyzed

by Rietveld refinement with the help of the RIETAN-2000 code [30]. The profile parameters were refined using the split-type Pearson VII function [31], and partial profile relaxation was applied to the diffraction peaks from the domain-wall planes. The values reported by Waasmaier and Kirfel [32] were used to correct for dispersion.

Time-of-flight secondary ion mass spectrometry (ToF-SIMS) data were acquired using a PHI TRIFT V nano TOF with a 30 keV Bi$_3^{++}$ primary ion source in pulsed mode. For each spectrum, the area analyzed is 50 × 50 μm. The mass resolution (m/Δm) typically exceeds 4000 for the (m/z) 27 peaks in the positive ion spectra. Positive ion spectra were mass calibrated using CH$_3^+$, C$_2$H$_5^+$, and C$_3$H$_7^+$ fragments.

For TEM analysis, the samples were cut into 3 mm in diameter discs, polished to a thickness of approximately 50 μm and dimpled to approximately 10 μm thick at the disc center. The specimens were prepared by ion milling with 2–4 keV Ar ions incident at an angle of 4° with respect to the normal to the sample surface. High-resolution TEM observations were made using a TOPCOM EM-002B TEM equipped with an energy dispersive X-ray spectrometer (EDS) with a 200 keV accelerating voltage. To acquire the SAD patterns, we used a 200 nm diameter aperture.

3. Results and discussions

3.1. KNN–NTK composite lead-free piezoelectric ceramic

3.1.1. Improvement of microstructure of KNN piezoelectric ceramic with NTK phase

Figure 2 shows SEM images of KNN–NTK composite lead-free piezoelectric ceramic and a Li-doped KNN single-phase ceramic [10] for comparison. As shown in **Figure 2a**, many voids approximately 10 μm in size appear in the Li-doped KNN ceramic. In contrast, such voids are rare in the image of the KNN–NTK composite ceramic in **Figure 2b**. By comparing these images, the effect of the NTK phase becomes clear; namely, the KNN–NTK composite lead-free piezoelectric ceramic forms a very dense surface with few voids.
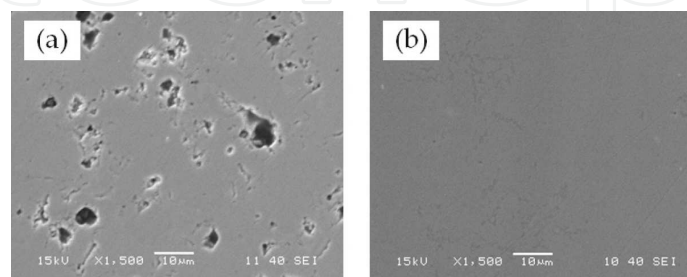

Figure 2. SEM images of polished surface of (a) Li-doped KNN prepared under common conditions and (b) KNN–NTK composite lead-free piezoelectric ceramic. Scale bar = 10 μm.
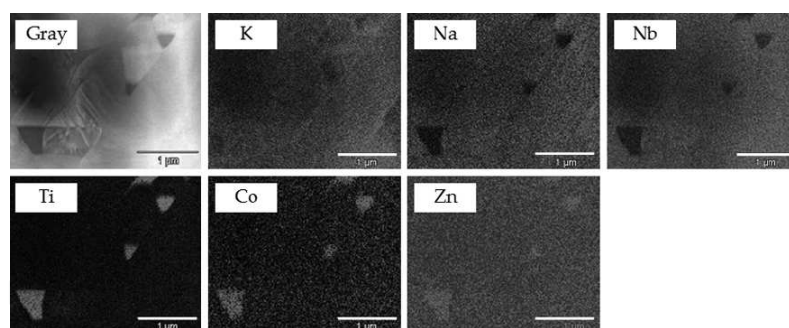
Figure 3. TEM-EDS elemental mapping, indicating the spatial distribution of K, Na, Nb, Ti, Co, and Zn in KNN–NTK composite lead-free piezoelectric ceramic. Scale bar = 1 μm.

Figure 3 shows TEM-EDS elemental mapping of the KNN–NTK composite ceramic. The Na map shows dice-like particles; these correspond to the KNN phase. The low-intensity area of the Na map seems to be voids. However, this area corresponds to the high-intensity area of the Ti map, that is, the low-intensity area of the Na map is not voids but correspond to the NTK phase. These results indicate that the voids are filled with the NTK phase. Furthermore, the high-intensity areas of the Co and Zn maps correspond to those of the Ti map, and the concentrations of the infinitesimal additives (e.g., Co and Zn) in the KNN phase are low.

Figure 4 shows an XRD pattern of the KNN–NTK composite ceramic. The small peaks marked with triangles, open circles, and closed circles in the enlarged view shown in **Figure 4b** are attributed to $KTiNbO_5$ (PDF#04-010-2961), $K_2(Ti,Nb,Co,Zn)_6O_{13}$ (PDF#00-039-0822), and $CoZnTiO_4$ (PDF#04-006-7279), respectively. The stoichiometric $KTiNbO_5$ is reported to be a dielectric material [33]. However, $KTi_{1-x}Nb_{1+x}O_5$, which contains oxygen defects, is reported to exhibit semiconducting behavior [34]. The NTK used in the present work is not a simple material; it was complexed with KNN and sintered under ambient atmosphere. Therefore, it must represent the settled ratio that forms at thermal equilibrium during sintering. $K_2(Ti,Nb,Co,Zn)_6O_{13}$ has a layered monoclinic structure $C2/m$, and $CoZnTiO_4$ has an inverse spinel-type structure [35]. Thus, a portion of the NTK phase must have transformed into $K_2(Ti,Nb,Co,Zn)_6O_{13}$ and/or $CoZnTiO_4$ by a reaction with Co and/or Zn solutes in the phase. However, tungsten bronze-type $Ba_2KNb_5O_{15}$ appeared in the specimens sintered under unsuitable conditions.
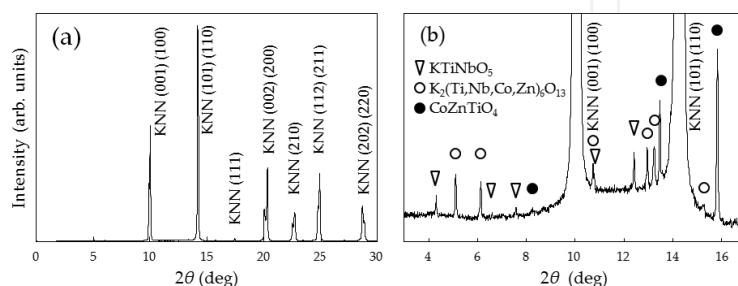

Figure 4. (a) XRD pattern from KNN–NTK composite ceramic and (b) enlarged view of panel (a).
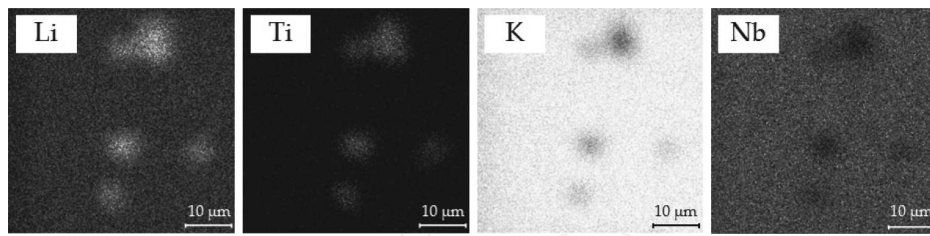
Figure 5. Positive ion images of KNN–NTK composite lead-free piezoelectric ceramic obtained by ToF-SIMS. Scale bar = 10 μm.

Li appears frequently in the KNN system. **Figure 5** shows positive ion images of the KNN–NTK composite ceramic obtained by ToF-SIMS. The high-intensity area corresponds to high element concentration. These images show that K and Nb have similar distributions, so the high-intensity areas in these images must correspond to the KNN phase. However, the image of Li is not the consistent with those of K and Nb, whereas the image of Li is similar to that of Ti. In other words, Li probably exists in KTiNbO$_5$, K$_2$(Ti,Nb,Co,Zn)$_6$O$_{13}$ and CoZnTiO$_4$. Therefore, at least for our materials, Li diffused out from the KNN phase, so less Li remains in the KNN phase than was put in when we blended it to make the KNN phases.

Figure 6a shows an annular bright-field STEM image of the NTK phase. The NTK phase has a layered structure; the K layer and the layer composed of Ti and Nb fall on a line. This elemental alignment corresponds to that of the KTiNbO$_5$ structure (see **Figure 1**). Therefore, we conclude that the NTK phase remains intact in KNN–NTK composite. **Figure 6b** shows a Cs-STEM image of a KNN/NTK interface. In general, in a material that consists of two or more phases, diffusion at the interface of the different phases directly deteriorates the electrical properties of the materials and must therefore be avoided. However, no intermediate phase is observed in the KNN/NTK interface region. Therefore, because of the difference between the formation temperatures of the phases, the NTK phase must have crystallized via epitaxial-like growth on the KNN crystal grain during sintering, so both phases are assumed to have adhered. The plane direction of a KNN/NTK interface is (001) or (100) and (001); that is, the NTK (001) plane grows on the KNN (001) or (100) plane.
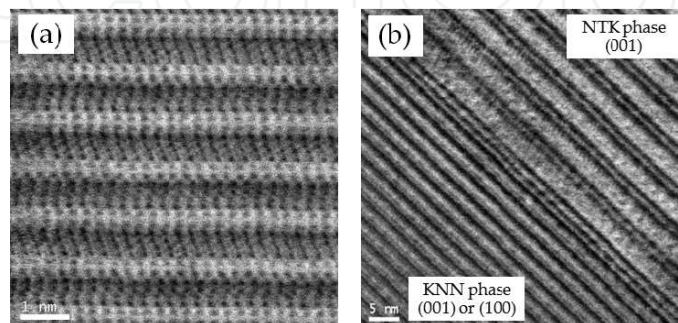

Figure 6. (a) STEM image of NTK phase, scale bar = 1 nm. (b) TEM image of NTK/KNN interface of KNN–NTK composite ceramic. Scale bar = 5 nm.

As previously mentioned, the NTK phase contains the additives. Thus, the absorption of these additives must have reacted with a portion of the NTK phase. The single phases of $KTiNbO_5$ and $CoZnTiO_4$ were sintered at 1100 and 1050°C, respectively [33, 35]. Therefore, they crystallized during cooling after the KNN phase was crystallized. This sintering reaction must have proceeded through the liquid-phase sintering.

The resistivity of the Li-doped KNN ceramic is 6.0×10^7 Ω cm [10], whereas that of the KNN–NTK composite ceramic is 3.6×10^{10} Ω cm. This KNN–NTK composite ceramic was polarized under a high voltage of 6 kV/mm. Because the voids are filled with the NTK phase, the electric field does not concentrate at the voids, resulting in improved polarizability.

3.1.2. Piezoelectric properties and productivity of KNN–NTK composite lead-free ceramic

KNN–NTK composite lead-free piezoelectric ceramic exhibits excellent piezoelectric properties, with the planar-mode electromechanical coupling coefficient $k_p = 0.52$ and the dielectric constant $\varepsilon_{33}^T/\varepsilon_0 = 1600$. The value of $\varepsilon_{33}^T/\varepsilon_0$ is equivalent to that of PZT, implying that the KNN–NTK composite ceramic is a suitable substitute for PZT. The piezoelectric properties of KNN–NTK composite ceramic are summarized in **Table 1**.

		KNN–NTK	MT-18K
Dielectric constant	$\varepsilon_{33}^T/\varepsilon_0$	1600	1450
Coupling coefficient	k_p	0.52	0.60
	k_t	0.41	0.41
	k_{33}	0.57	0.72
	k_{31}	0.29	0.34
	k_{15}	0.48	0.54
Piezoelectric constant (pC/N)	d_{33}	240	340
	d_{31}	104	142
	d_{15}	312	300
Frequency constant (Hz m)	N_p	3170	2200
	N_t	2940	2150
	N_{33}	2210	1500
	N_{31}	2220	1650
	N_{15}	1420	1300
Elastic compliance coefficient (pm²/N)	s_{33}^E	12.0	15.7
Dielectric loss (%)	tan δ	1.9	0.4
Mechanical quality factor	Qm	88	1800
Density (g/cm³)	ρ	4.54	7.60
Curie temperature (°C)	Tc	290	300

Table 1. Piezoelectric properties of KNN–NTK composite lead-free piezoelectric ceramic and of MT-18K (Navy Type I PZT, NGK Spark Plug Co., Ltd.).

Figure 7 shows the planar-mode resonance characteristics of a KNN–NTK composite ceramic disc. The maximum phase angle θ is 86°, and sufficient phase inversion is observed. The elastic compliance coefficient s_{33}^{E} of 12 pm^2/N is much smaller than that for conventional PZT. This small elastic compliance coefficient causes the piezoelectric constant d_{33} of KNN–NTK composite ceramic to be less than that of the conventional PZT.

However, the mechanical quality factor for KNN–NTK composite ceramic is $Qm = 88$, which is almost the same as that of the conventional Navy Type II PZT. Other characteristics of KNN–NTK composite ceramic include the frequency constant N_p of 3170 Hz m, which is about 50% greater than that of conventional PZT, and the density, which is fairly less than that of conventional PZT. These characteristics of KNN-based piezoelectric ceramic deserve attention.
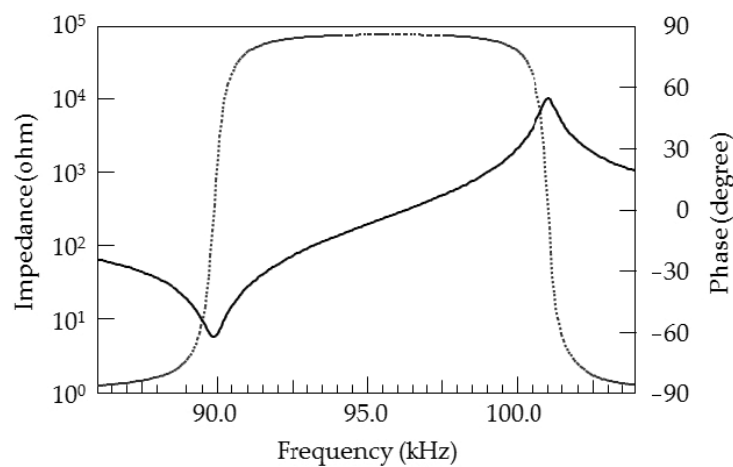

Figure 7. Planar-mode resonance characteristics of KNN–NTK lead-free piezoelectric ceramic disc of 35 mm in diameter and 2 mm in thick. Impedance magnitude is drawn as a solid line, and phase angle is drawn as a dotted line.

Figure 8 shows the dielectric constant $\varepsilon_{33}^{T}/\varepsilon_0$ and the coupling coefficient k_p as a function of temperature between −50 and 350°C. The Curie temperature Tc of the KNN–NTK composite ceramic is 290°C, which is equivalent to that of conventional PZT. For comparison, **Figure 8** also shows the dielectric constant of MT-18K (Navy Type I PZT, NGK Spark Plug Co., Ltd.) near room temperature. In the practical temperature range from 0 to 150°C, the rate of change of the dielectric constant of MT-18K exceeds 80%, whereas that of the KNN–NTK composite ceramic is less than 10%. The temperature dependence of the dielectric constant of KNN–NTK composite ceramic is thus much weaker than that of Navy Type I PZT MT-18K. Consequently, the thermal stability of KNN–NTK composite ceramic is confirmed, and its Tc is sufficiently high to satisfy the requirements for in-vehicle applications. After 1000 temperature cycles between −40 and 150°C, the rate of the piezoelectric constant d_{33} of KNN–NTK composite ceramic decreased by less than 2%, which compares favorably with that of 10% for MT-18K. Therefore, this KNN–NTK composite ceramic offers an advantage for sensor applications. Furthermore, the dielectric constant of this KNN–NTK composite ceramic does not significantly vary within the practical temperature range that is common in conventional KNN piezoelectric ceramics.

Figure 9 shows the aging properties of the coupling coefficient k_p and the frequency constant N_p of KNN–NTK composite ceramic. The same parameters of Navy Type I PZT MT-18K are also shown. To facilitate comparison, the initial values are normalized to unity. The rate of deterioration in the coupling coefficient k_p of MT-18K was approximately 7% after the sample was aged by polarization for 1000 days, whereas k_p of the KNN–NTK composite ceramic decreases by approximately 4% under the same conditions. As found for these aging characteristics, k_p of KNN–NTK composite ceramic ages better than that of MT-18K. Similarly, the frequency constant N_p of MT-18K increases by approximately 2% upon similar aging, whereas that of KNN–NTK composite ceramic remains unchanged, indicating that N_p for KNN–NTK composite ceramic is extremely stable.
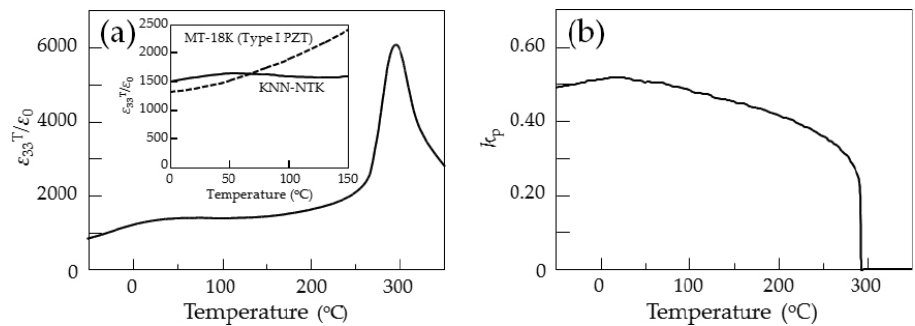

Figure 8. Temperature dependence of (a) dielectric constant $\varepsilon_{33}^T/\varepsilon_0$ and (b) planar-mode electromechanical coupling coefficient k_p of KNN–NTK composite piezoelectric ceramic.
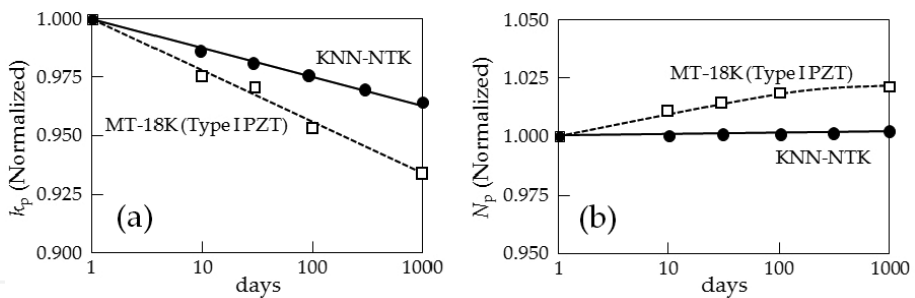

Figure 9. Aging characteristics of (a) planar-mode electromechanical coupling coefficient k_p, and (b) frequency constant N_p of KNN–NTK composite lead-free piezoelectric ceramic, comparing with Navy Type I PZT MT-18K.

Bending strength (MPa)	117
Vickers hardness (N/mm²)	518
Young's modulus (GPa)	100
Poisson's ratio	0.36
Thermal conductivity (W/m K)	2.5

Table 2. Mechanical properties of KNN–NTK composite lead-free piezoelectric ceramic.

The mechanical properties of KNN–NTK composite ceramic are summarized in **Table 2**. The bending strength of KNN–NTK composite ceramic is 117 MPa, which exceeds that of MT-18K of 100 MPa. All mechanical properties of KNN–NTK composite lead-free piezoelectric ceramic are equal or exceed those of conventional PZT.

Mass production is also an important factor for commercialization. We scaled the manufacturing process to 100 kg per batch for granulated ceramic powder using a spray-drying technique (**Figure 10a**). The calcination process is very important for obtaining high-quality spray-drying powder. Piezoelectric elements in the form of 70 mm in diameter, 10 mm in thick discs were prepared from these powders. Furthermore, we conducted durability tests of a knocking sensor fabricated with this KNN–NTK composite lead-free piezoelectric ceramic (**Figure 10b**). The results showed that the durability of the sensor fabricated with the KNN–NTK composite was equal or superior to that of the sensor fabricated with PZT. Moreover, the output level of KNN–NTK composite-based sensor almost approaches that the PZT-based sensor. We confirmed that the resulting KNN–NTK composite lead-free piezoelectric ceramic still had attractive piezoelectric properties.
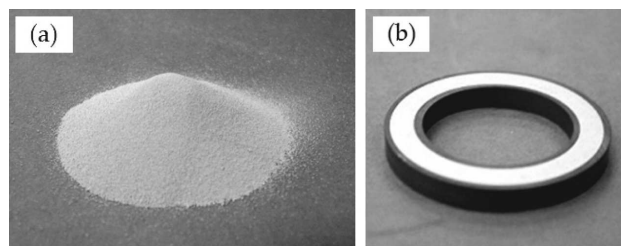

Figure 10. (a) Granulated powder for KNN–NTK composite lead-free piezoelectric ceramic. (b) KNN–NTK composite lead-free piezoelectric ceramic element for knocking sensor.

3.2. Improvement of KNN–NTK composite lead-free piezoelectric ceramic with two-phase coexisting state

3.2.1. Tetragonal and orthorhombic two-phase coexisting state in the KNN–NTK composite lead-free piezoelectric ceramic

To improve the piezoelectric properties, we analyze in detail the crystal structure and phase transition. **Figure 11** shows XRD patterns as a function of 2θ from 14° to 22° for pulverized samples of KNN–NTK composite lead-free piezoelectric ceramic and with a magnified intensity scale. The strong peaks at $2\theta = 14.2°$, 17.4°, and 20.2° correspond to the Miller indices of the KNN phase (110_{pc}, 111_{pc}, and 200_{pc}, respectively) with perovskite-type structure. Here, the subscript "pc" refers to the pseudo-cubic cell. Weak peaks marked by solid circles in **Figure 11** are assigned to CoZnTiO$_4$, which has an inverse spinel-type structure. The Miller indices for these peaks are 311, 222, and 400, respectively. Throughout the range $0.33 \leq x \leq 0.75$, the intensities of the weak peaks are almost unchanged. We suggest that the formation of CoZn-TiO$_4$ depends on the element and the amount of additives but is independent of the Na fraction.
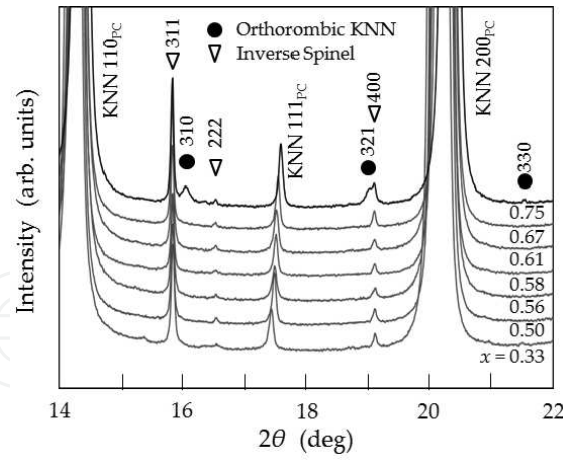
Figure 11. XRD patterns of $K_{1-x}Na_xN–NTK$ composite lead-free piezoelectric ceramic in 2θ range from 14° to 22°, diffraction peaks of orthorhombic phase are can be seen only at $x = 0.75$.

All main diffraction peaks in the XRD patterns are attributed to the perovskite-type structure. These peaks appear for $0.33 \leq x \leq 0.67$ and are attributed to the tetragonal KNN system, which is known as the high temperatures stable structure of undoped KNN [20]. Assuming $P4mm$ symmetry, the Rietveld refinement fits significantly better compared with the results obtained upon assuming the ideal cubic perovskite-type structure. The R-values of the Rietveld refinements are $R_I = 3.6–4.8\%$ and $R_F = 1.8–2.2\%$ for the $P4mm$ tetragonal model, whereas $R_I = 6.1–12.8\%$ and $R_F = 3.6–7.0\%$ for the $Pm–3m$ cubic model. The results of the XRD analysis show that KNN for $0.33 \leq x \leq 0.67$ is a single-phase tetragonal system and likely belongs to the $P4mm$ symmetry. Assuming that $P4mm$ symmetry restricts the displacement of the atoms to be along the c axis, the NbO_6 octahedra permit no tilting, so the tilt system should be expressed by the Glazer notation $a^0a^0c^0$ [36].

The main features of the XRD pattern for $x = 0.75$ do not significantly change compared with those for $x \leq 0.67$. However, the XRD pattern for $x = 0.75$ shows weak peaks that cannot be assigned to the tetragonal system with $a^0a^0c^0$. Ahtee and Glazer suggested that the crystallographic symmetry of undoped Na-rich (ca. $0.75 < x < 0.9$) KNN ceramic at temperatures ranging from 200 to 400°C belongs to the $Imm2$ space group ($a^+b^+c^0$ system) [20, 21], whereas Baker et al. [23] suggested that the symmetry belongs to the $Amm2$ space group ($a^+b^0c^0$ system). We hypothesize that Na-rich KNN has $Imm2$ symmetry with an $a^+b^+c^0$ tilt system on the structure refinement because the optimized lattice constants of the pseudo-cubic cell indicate that this assignment is more appropriate. The weak peaks are attributed to the $Imm2$ orthorhombic phase, which has the tilting of the NbO_6 octahedra. The Miller indices for these peaks are {310}, {321}, and {330}. This orthorhombic structure has double lattice constants, which are represented by the $2 \times 2 \times 2$ superlattice setting in the pseudo-cubic cell.

Assuming the combination of $P4mm$ tetragonal and $Imm2$ orthorhombic structures, the XRD patterns for $x = 0.75$ are fit by two-phase Rietveld refinement. The overall R-factor is estimated to be $R_P = 5.87\%$ with the two-phase model, whereas at best $R_P = 6.96\%$ with the single-phase

*P*4*mm* model. The lattice constants of the orthorhombic structure are estimated to be $a = 7.88875$ Å, $b = 7.93082$ Å, and $c = 7.96895$ Å.
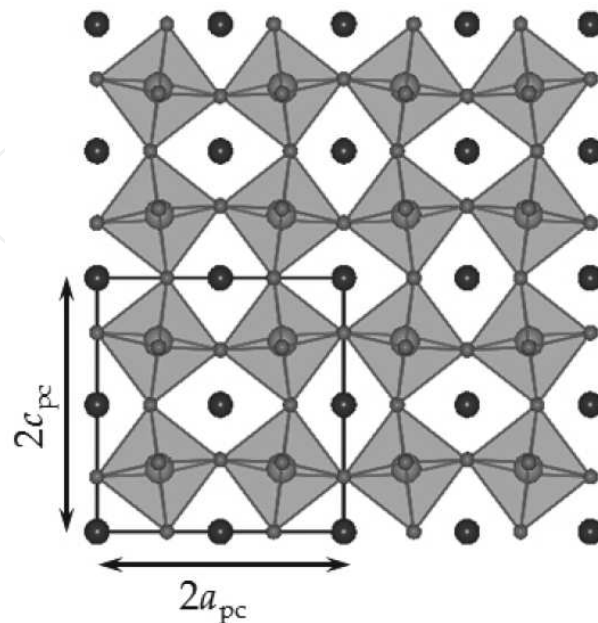

Figure 12. Structure model of *Imm*2 orthorhombic phase projected along the [100] direction for $x = 0.75$.

Figure 12 shows a structural model of *Imm*2 projected along the [010] direction. This orthorhombic structure has tilt ordering of the NbO$_6$ octahedra, where $2 \times 2 \times 2$ *Immm* symmetry is predicted without deformation of the NbO$_6$ octahedra. The NbO$_6$ octahedra are likely to be simultaneously deformed and tilted in the *Imm*2 phase of this composite system. Note that because *Imm*2 is a noncentrosymmetric space group, it allows polarization; in contrast, because *Immm* is a centrosymmetric space group, it forbids polarization. The structural details optimized by the Rietveld refinement will be discussed in another presentation.

Figure 13 shows the cell volume and tetragonality ratio c/a of the primary tetragonal phase calculated from the dimensions of the crystal unit cell. It also shows the dielectric polarization P estimated from the point-charge model with the formal charges of the ions located at positions optimized by the Rietveld refinements. The cell volume monotonically decreases with increasing Na fraction x, which is caused by the decrease in effective ionic radius upon replacing K$^+$ with Na$^+$. However, the rate of decline increases in the range $x > 0.56$. At $x = 0.75$, the cell volume 62.01 Å^3 of the primary tetragonal phase approaches that of the pseudo-cubic cell of the secondary orthorhombic phase 62.32 Å^3. The tetragonality ratio of the tetragonal phase is estimated to lie between 1.010 and 1.012 for $0.33 \leq x \leq 0.67$, and to be 1.006 for $x = 0.75$. The value defined by $2c/(a + b)$ for the secondary orthorhombic phase is estimated to be 1.007 for $x = 0.75$, which is close to the tetragonality ratio c/a of the primary phase of this composition. We hypothesize that the maximum value of the tetragonality ratio occurs around $x = 0.50$. However, the estimated dielectric polarization P increases gradually for $0.33 \leq x \leq 0.50$ and drops sharply for $0.67 \leq x \leq 0.75$.
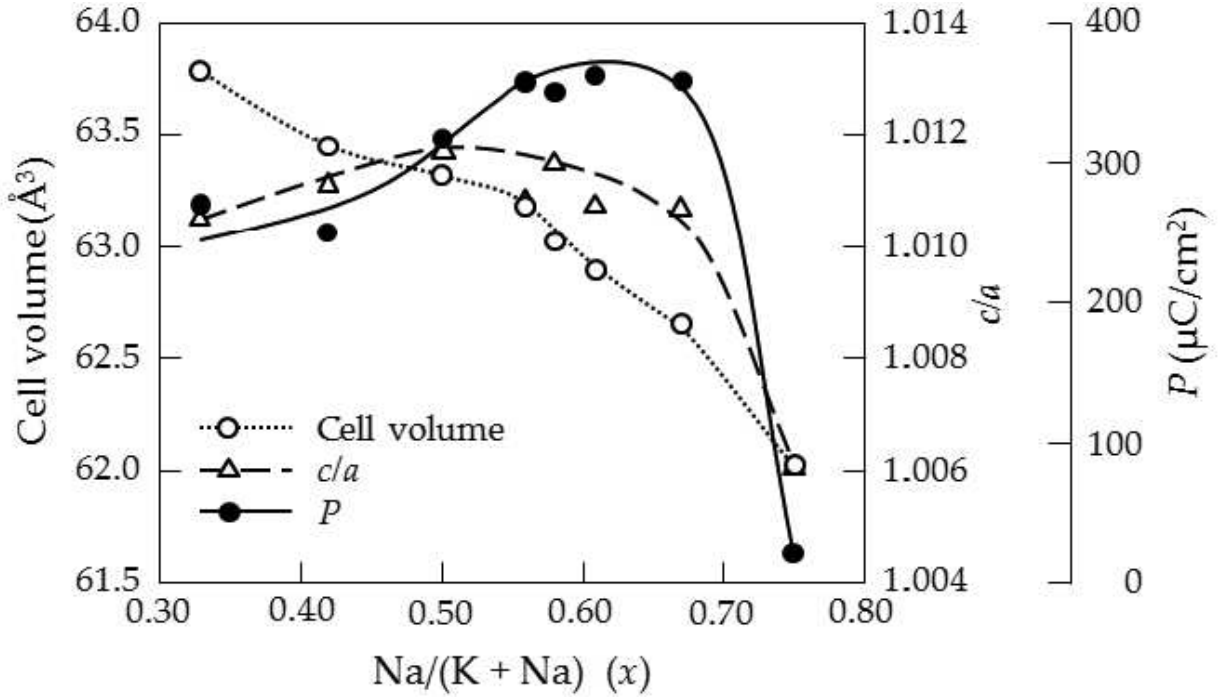
Figure 13. Comparison of cell volume, tetragonality ratio c/a, and dielectric polarization P of $K_{1-x}Na_xN$–NTK composite lead-free piezoelectric ceramic as a function of Na fraction x. Sample for $x = 0.75$ gives the values of the primary tetragonal phase.

The maximum value of 363 $\mu C/cm^2$ is about an order of magnitude larger than that of un-doped KNN [37]. These results suggest that the dielectric polarization P cannot be correlated with the tetragonality ratio. Note that the discrepancy between P and the tetragonality ratio has also been reported, for a PZT system [38].

The structural information obtained from XRD is dominated by the structure averaged over the macroscopic volume. In other words, it is not sensitive to identify the microstructure of ceramic. In this study, TEM was used to investigate the KNN–NTK composite ceramic microstructure.

Figure 14 shows SAD patterns obtained from a single grain of KNN in the KNN–NTK composite ceramic. The top row shows $[100]_{pc}$ and the bottom row shows $[210]_{pc}$ zone-axis SAD patterns. From left to right, the panels correspond to $x = 0.33, 0.56, 0.58, 0.67,$ and 0.75, respectively. The 001_{pc}, 011_{pc}, and $1\text{–}20_{pc}$ reflections appear in all SAD patterns for $0.33 \le x \le 0.75$. The SAD patterns for $x = 0.33$ consist only of these spots, which conforms to the single-phase model that we derive from the Rietveld refinement. However, superlattice reflections are observed for $x = 0.56, 0.58, 0.67,$ and 0.75. The slanted and vertical arrows in **Figure 14c**, **e–j** indicate the directions indexed by 011 and 1–21 based on the 2 × 2 × 2 superlattice unit cell. However, the SAD patterns in **Figure 14h**, **j** exhibit very weak spots (sideways arrows) that cannot be assigned to the 2 × 2 × 2 superlattice structure.
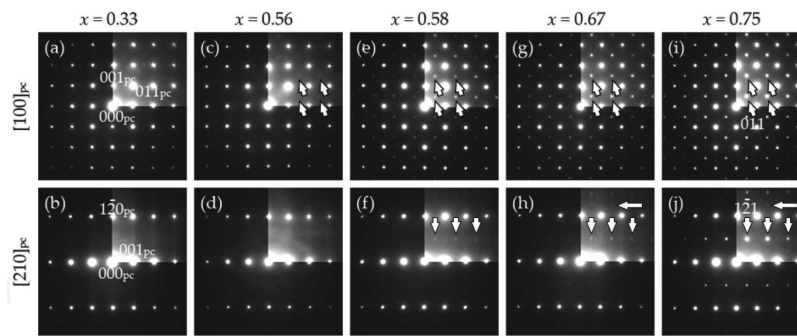
Figure 14. SAD patterns of (a) [100]$_{pc}$ and (b) [210]$_{pc}$ zone-axis for x = 0.33, (c) [100]$_{pc}$ and (d) [210]$_{pc}$ zone-axis for x = 0.56, (e) [100]$_{pc}$ and (f) [210]$_{pc}$ zone-axis, (g) [100]$_{pc}$ and (h) [210]$_{pc}$ zone-axis for x = 0.67, (i) [100]$_{pc}$ and (j) [210]$_{pc}$ zone-axis for x = 0.75. The spots marked by slanted and vertical arrows are superlattice reflections based on the 2 × 2 × 2 superlattice unit cell.

Although the peaks of the 2 × 2 × 2 superlattice phase do not appear in the XRD patterns for x = 0.58 and 0.67, TEM analysis indicates that the superlattice phase of KNN does exist at these Na fractions, in the same way as they do for x = 0.75. The SAD pattern for x = 0.56 shows broad and dim superlattice reflections, which suggest that a short coherent length for the structural modulation. We believe that the KNN phase of the KNN–NTK composite lead-free piezoelectric ceramic around x = 0.56 consists of a two-phase coexisting state. According to the Rietveld refinement discussed above, the weight fraction of the superlattice phase is estimated to be 44.2 wt% for x = 0.75. In the K$_{1-x}$Na$_x$N–NTK system, the tetragonal and orthorhombic phases of KNN coexist for $x \geq$ 0.56, with the volume fraction of the orthorhombic phase gradually increases with increasing Na fraction x.

If the secondary superlattice phase of KNN that exists for x = 0.56, 0.58, 0.67, and 0.75 has the tilt-ordered structure, the weak spots can naturally be assigned to the 1/2\{$hh0$\}$_{pc}$ (h: odd) planes, whereas such spots are not observed for the primary *P4mm* tetragonal phase. We calculated the Fourier transforms (FT) of the HR-TEM images (i.e., extracted the 1/2\{110\}$_{pc}$ spots) and synthesized the dark-field images using the inverse FT of the extracted peaks.

Figure 15a–c show the results of the inverse FT treatment of the HR-TEM images of samples for x = 0.58, 0.67, and 0.75. In the images, the brighter areas correspond to the superlattice phase. We also applied EDS to the dark and bright areas to confirm that the contrast is not caused by the compositional segregation within the local area. The probe has a diameter of approximately 1.0 nm. The contrast shown in the inverse FT-treated images suggests that the tilt ordering of the superlattice phase is confined within the granular nanodomains dispersed in the tetragonal matrix. The granular nanodomains gradually increase with x for 0.58 ≤ x ≤ 0.67, and an abrupt increase and agglomeration is observed at x = 0.75. The formation of the superlattice structure with the tilting of the NbO$_6$ octahedra is probably caused by the reduction in cell volume with increasing of the smaller Na$^+$ radius in the large x region. Considering the XRD, SAD, and FT-treated HR-TEM results, the primary phase of the KNN belongs to 1 × 1 × 1 tetragonal structure, whereas the secondary phase belongs to a 2 × 2 × 2 orthorhombic structure with the tilt ordering of the NbO$_6$ octahedra.
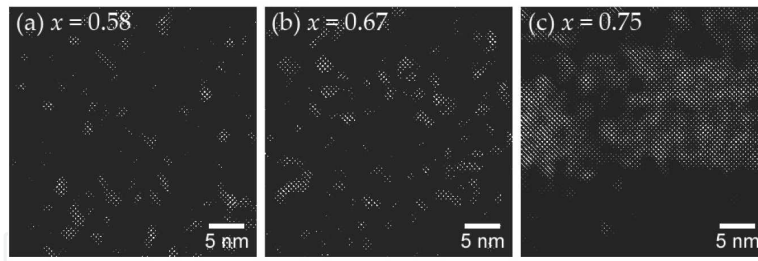
Figure 15. Inverse FT-treated HR-TEM images for (a) x = 0.58, (b) x = 0.67, and (c) x = 0.75, where the brighter area corresponds to the 2 × 2 × 2 *Imm*2 orthorhombic phase and the darkness areas correspond to the tetragonal phase matrix. Scale bar = 5 nm.

3.2.2. Phase transition and piezoelectric properties of KNN–NTK composite lead-free piezoelectric ceramic

Figure 16 shows the dielectric constant $\varepsilon_{33}^{T}/\varepsilon_0$ and the coupling coefficient k_p as a function of the Na fraction x. The $\varepsilon_{33}^{T}/\varepsilon_0$ is almost constant for $0.33 \leq x \leq 0.56$, then increases slightly for $0.56 < x \leq 0.67$, and finally drops sharply to lower values for $0.67 < x \leq 0.75$. The behavior of $\varepsilon_{33}^{T}/\varepsilon_0$ is similar to that of the dielectric polarization P (see **Figure 13**).

The enhanced piezoelectric properties of PZT near the MPB composition are suggested to mainly originate from the polarization rotation rather than from the formation of nanodomains [28]. However, the coexistence in a PZT system of the tetragonal structure with <001> polarization and the rhombohedral structure with <111> polarization can still be correlated with easier rotation of the polarization direction, because it indicates the similar free energies of the two phases and a lower energy barrier for polarization rotation. In our KNN–NTK composite lead-free piezoelectric ceramic, we observe the coexistence of orthorhombic nanodomains dispersed in the tetragonal matrix over a wide range of Na fraction for $0.56 \leq x \leq 0.67$. This result suggests a reduction in the energy barrier when the structure transforms from tetragonal to orthorhombic, and vice versa, and easier rotation of the polarization from [001] to [010], which may be assisted by the formation of the intermediate orthorhombic structure with small polarization in this compositional range.
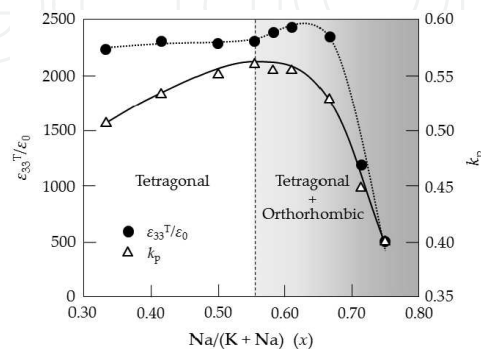

Figure 16. Phase transition and piezoelectric properties of K$_{1-x}$Na$_x$N–NTK composite lead-free piezoelectric ceramic as a function of Na fraction x.

The dielectric polarization P, calculated from the atomic positions optimized for the orthorhombic phase at $x = 0.75$, is 1.28 μC/cm^2. The decrease in the dielectric constant $\varepsilon_{33}^T/\varepsilon_0$ around $x = 0.75$ is partly related to the decrease in the tetragonal phase that results from the increase in the orthorhombic phase. The P of the orthorhombic phase is more than two orders of magnitude lower than that of the tetragonal phase.

In contrast, the coupling coefficient k_p gradually increases with increasing x for $0.33 \leq x \leq 0.56$, reaches a maximum of 0.56 near $x = 0.56$, and then decreases with increasing x for $x \geq 0.67$. This behavior differs from that of the dielectric constant $\varepsilon_{33}^T/\varepsilon_0$ or the dielectric polarization P, but resembles the behavior of the tetragonality ratio. The deterioration of k_p for $x > 0.56$ is naturally related to the smaller tetragonality ratio in this region.

The point $x = 0.56$ at which the maximum coupling coefficient k_p occurs corresponds to the minimum value of x at which the orthorhombic phase is generated. However, the highest dielectric constant occurs near $x = 0.60$, where the two-phase coexists progressed state. We thus conclude that this KNN–NTK composite lead-free piezoelectric ceramic exhibits excellent piezoelectric properties because of the two-phase coexisting state.

The phase transition of the KNN–NTK composite piezoelectric ceramic occurs gently, and the orthorhombic and tetragonal phases coexist in the KNN for a wide range of $x > 0.56$. In this way, this phase transition differs from the drastic phase transition at the MPB in PZT. This gentle transition is similar to the behavior of a relaxor. To verify the relaxation degree, we estimated the relaxor ferroelectricity of the KNN–NTK composite lead-free piezoelectric ceramic in the two-phase coexisting state.
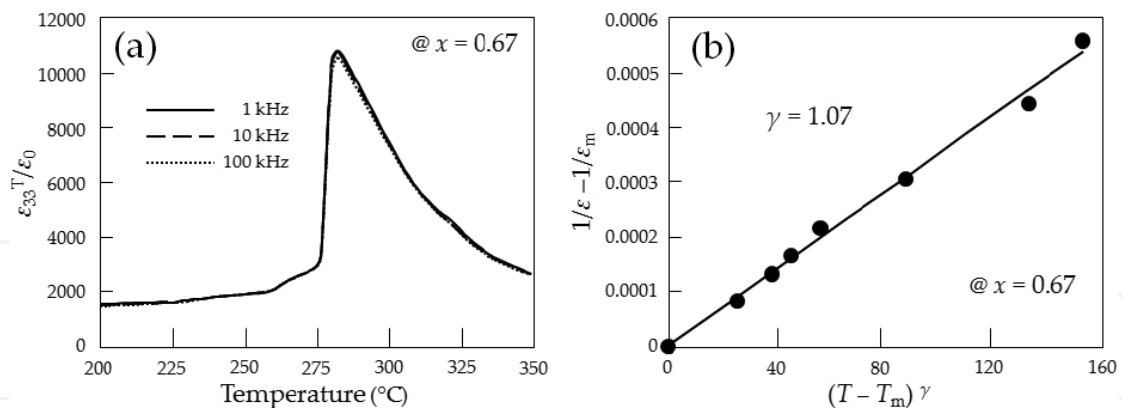

Figure 17. (a) Temperature dependences of dielectric constant of K$_{1-x}$Na$_x$N–NTK composite lead-free piezoelectric ceramic at 1 kHz (solid line), 10 kHz (dashed line), and 100 kHz (dotted line) for $x = 0.67$. (b) Behavior of inverse dielectric constant $(1/\varepsilon - 1/\varepsilon_m)$ as a function of $(T - T_m)^{\gamma}$.

Figure 17a shows the dielectric constant of K$_{1-x}$Na$_x$N–NTK composite lead-free piezoelectric ceramic as a function of temperature around Tc at frequency of 1, 10, and 100 kHz for $x = 0.67$. The dielectric constant hardly decreases with increasing frequency. Relatively sharp peaks corresponding to Tc appear around 280°C, but Tc does not shift as a function of frequency.

The diffuseness can be described by a modified Curie–Weiss law [39],

$$\frac{1}{\varepsilon} - \frac{1}{\varepsilon_\mathrm{m}} = \frac{\left(T - T_\mathrm{m}\right)^{\gamma}}{C} \qquad (1)$$

where γ is the diffusivity of dielectric relaxation, ranging from 1 for a normal ferroelectric to 2 for a relaxor ferroelectric. C is Curie constant, and T_m is the temperature at which the dielectric constant reaches its maximum ε_m. **Figure 17b** shows the inverse dielectric constant as a function of temperature at 100 kHz using $K_{1-x}Na_xN$–NTK composite ceramic for $x = 0.67$, at which the highest dielectric constant is obtained. The diffusivity constant γ estimated by a linear fit is 1.07. As γ approaches unity, the KNN–NTK composite ceramic exhibits normal ferroelectricity. These results indicate that the KNN–NTK composite lead-free piezoelectric ceramic is not a relaxor.

4. Conclusions

We developed $K_{1-x}Na_xN$–NTK composite lead-free piezoelectric ceramic composed of the two primary phases KNN and NTK. The NTK phase is a dielectric substance with a layered structure and is not piezoelectric. This phase fills the voids between KNN crystalline particles, and a portion of this phase transforms into $K_2(Ti,Nb,Co,Zn)_6O_{13}$ and/or $CoZnTiO_4$. Consequently, a densely sintered ceramic is obtained. This KNN–NTK composite lead-free piezoelectric ceramic exhibits enhanced piezoelectric characteristics, such as a planar-mode electromechanical coupling coefficient $k_\mathrm{p} = 0.52$, a dielectric constant $\varepsilon_{33}^\mathrm{T}/\varepsilon_0 = 1600$, $N_\mathrm{p} = 3170$ Hz m, and a high thermal durability.

In this system, KNN forms the single tetragonal phase for $x < 0.56$. However, near $x = 0.56$ appears a two-phase coexisting state containing both the $P4mm$ tetragonal phase and the $Imm2$ orthorhombic phase, and the fraction of the orthorhombic phase increases with x. No XRD peaks corresponding to the $Imm2$ orthorhombic phase are observed for the initial coexisting state; however, superlattice reflections appear in the SAD patterns. This $K_{1-x}Na_xN$–NTK composite lead-free piezoelectric ceramic, with granular $Imm2$ orthorhombic nanodomains dispersed in a $P4mm$ tetragonal matrix, has excellent piezoelectric properties, with a planar-mode electromechanical coupling coefficient $k_\mathrm{p} = 0.56$ at the onset of the two-phase coexisting state. The phase transition of $K_{1-x}Na_xN$–NTK composite lead-free piezoelectric ceramic occurs gently, which distinguishes it from the drastic phase transition of the MPB of PZT. However, the diffusivity γ of $K_{1-x}Na_xN$–NTK shows that $K_{1-x}Na_xN$–NTK composite lead-free piezoelectric ceramic is close to a ferroelectric but is not a relaxor.

Acknowledgements

Author details

Kazushige Ohbayashi

Address all correspondence to: k-obayashi@mg.ngkntk.co.jp

NGK Spark Plug Co., Ltd., Iwasaki, Komaki, Aichi, Japan

References

[1] Li E, Kakemoto H, Hoshina T, Tsurumi T. A shear-mode ultrasonic motor using potassium sodium niobate-based ceramics with high mechanical quality factor. Jpn. J. Appl. Phys. 2008;Part 1 47:7702.

[2] Li E, Sasaki R, Hoshina T, Takeda H, Tsurumi T. Miniature ultrasonic motor using shear mode of potassium sodium niobate-based lead-free piezoelectric ceramics. Jpn. J. Appl. Phys. 2009;Part 1 48:09KD11.

[3] Kawada S, Kimura M, Higuchi Y, Takagi H. (K,Na)NbO$_3$-based multilayer piezoelectric ceramics with nickel inner electrodes. Appl. Phys. Express. 2009;2:111401.

[4] Tsurumi T, Takeda H, Li E, Hoshina T. Devices using shear mode of lead-free piezo-electric ceramics. Mater. Integr. 2009;22:25 (in Japanese).

[5] Tanuma C. Development of an inkjet head using lead-free piezoelectric ceramics. J. Jpn. Soc. Colour Mater. 2013;86:93 (in Japanese).

[6] Kwok KW, Lee T, Choy SH, Chan HLW. Lead-free piezoelectric transducers for microelectronic wirebonding applications. In: Ernesto SG, editor. Piezoelectric Ceramics. Rijeka: InTech; 2010. pp. 145–164.

[7] Jaeger RE, Egerton L. Hot pressing of potassium–sodium niobates. J. Am. Ceram. Soc. 1962;45:209.

[8] Saito Y, Takao H, Tani T, Nonoyama T, Takatori K, Homma T, Nagaya T, Nakamura M. Lead-free piezoceramics. Nature 2004;432:84.

[9] Hatano K, Doshida Y, Mizuno Y. Microstructural design and piezoelectric properties of Na$_{0.5}$K$_{0.5}$NbO$_3$ ceramics. J. Jpn. Soc. Powder Powder Metall. 2012;59:507 (in Japanese).

[10] Matsuoka T, Kozuka H, Kitamura K, Yamada H, Kurahashi T, Yamazaki M, Ohbayashi K. KNN–NTK composite lead-free piezoelectric ceramic. J. Appl. Phys. 2014;116:154104.

[11] Yamada H, Matsuoka T, Kozuka H, Yamazaki M, Ohbayashi K, Ida T. Improvement of the piezoelectric properties in (K,Na)NbO$_3$-based lead-free piezoelectric ceramic with two-phase co-existing state. J. Appl. Phys. 2015;117:214102.

[12] Zuo R, Fang X, Ye C, Li L. Phase transitional behavior and piezoelectric properties of lead-free $(Na_{0.5}K_{0.5})NbO_3$–$(Bi_{0.5}K_{0.5})TiO_3$. Ceram. J. Am. Ceram. Soc. 2007;90:2424.

[13] Du H, Zhou W, Luo F, Zhu D, Qu S, Li Y, Pei Z. Design and electrical properties' investigation of $(K_{0.5}Na_{0.5})NbO_3$–$BiMeO_3$ lead-free piezoelectric ceramics. J. Appl. Phys. 2008;104:034104.

[14] Wu J, Xiao D, Wang Y, Wu W, Zhang B, Zhu J. Improved temperature stability of CaTiO3-modified $[(K_{0.5}Na_{0.5})_{0.96}Li_{0.04}](Nb_{0.91}Sb_{0.05}Ta_{0.04})O_3$ lead-free piezoelectric ceramics. J. Appl. Phys. 2008;104:024102.

[15] Lin D, Guo MS, Lam KH, Kwok KW, Chan HLW. Lead-free piezoelectric ceramic $(K_{0.5}Na_{0.5})NbO_3$ with MnO_2 and $K_{5.4}Cu_{1.3}Ta_{10}O_{29}$ doping for piezoelectric transformer application. Smart Mater. Struct. 2008;17:035002.

[16] Tanaka T, Hayashi H, Kakimoto K, Ohsato H, Iijima I. Effect of (Na,K)-excess precursor solutions on alkoxy-derived $(Na,K)NbO_3$ powders and thin films. Jpn. J. Appl. Phys. 2007;Part 1 46:6964.

[17] Skidmore TA, Milne SJ. Phase development during mixed-oxide processing of a $[Na_{0.5}K_{0.5}NbO_3]_{1-x}$–$[LiTaO_3]_x$ powder. J. Mater. Res. 2007;22:2265.

[18] Skidmore TA, Comyn TP, Milne SJ. Temperature stability of $([Na_{0.5}K_{0.5}NbO_3]_{0.5}$–$[LiTaO_3]_{0.07})$ lead-free piezoelectric ceramics. Appl. Phys. Lett. 2009;94:222902.

[19] Mgbemere HE, Herber R, Schneider GA. Effect of MnO_2 on the dielectric and piezoelectric properties of alkaline niobate based lead free piezoelectric ceramics. J. Eur. Ceram. Soc. 2009;29:1729.

[20] Ahtee M, Glazer AM. Lattice parameters and tilted octahedra in sodium–potassium niobate solid solutions. Acta Cryst. 1976;A 32:434.

[21] Ahtee M, Hewat AW. Structural phase transition in sodium–potassium niobate solid solutions by neutron powder diffraction. Acta Cryst.1978;A 34:309.

[22] Baker DW, Thomas PA, Zhang N, Glazer AM. Structural study of $K_xNa_{1-x}NbO_3$ (KNN) for compositions in the range $x = 0.24$–0.36. Acta Cryst. 2009;B 65:22.

[23] Baker DW, Thomas PA, Zhang N, Glazer AM. A comprehensive study of the phase diagram of $K_xNa_{1-x}NbO_3$. Appl. Phys. Lett. 2009;95:091903.

[24] Zang GZ, Wang JF, Chen HC, Su WB, Wang CM, Qi P, Ming BQ, Du J, Zheng LM, Zhang S, Shrout TR. Perovskite $(Na_{0.5}K_{0.5})_{1-x}(LiSb)_xNb_{1-x}O_3$ lead-free piezoceramics. Appl. Phys. Lett. 2006;88:212908.

[25] Guo Y, Kakimoto K, Ohsato H. Phase transitional behavior and piezoelectric properties of $(Na_{0.5}K_{0.5}) NbO_3$–$LiNbO_3$ ceramics. Appl. Phys. Lett. 2004;85:4121.

[26] Rubio-Marcos F, Navarro-Rojero MG, Romero JJ, Marchet P, Fernandez JF. Piezoceramics properties as a function of the structure in the system (K,Na,Li)(Nb,Ta,Sb)O$_3$. IEEE Trans. Ultrason. Ferroelectr. Freq. Control. 2009;56:1835.

[27] Rubio-Marcos F, Romero JJ, Fernandez JF, Marchet P. Control of the crystalline structure and piezoelectric properties of (K,NaLi)(Nb,Ta,Sb)O$_3$ ceramics through transition metal oxide doping. Appl. Phys. Express. 2011;4:10150.

[28] Dai YJ, Zhang XW, Chen KP. Morphotropic phase boundary and electrical properties of K$_{1-x}$Na$_x$NbO$_3$ lead-free ceramics. Appl. Phys. Lett. 2009;94:042905.

[29] Karaki T, Katayama T, Yoshida K, Maruyama S, Adachi M. Morphotropic phase boundary slope of (K,Na,Li)NbO$_3$–BaZrO$_3$ binary system adjusted using third component (Bi,Na)TiO$_3$ additive. Jpn. J. Appl. Phys. 2013;52:09KD11.

[30] Izumi F, Ikeda T. A Rietveld-Analysis Programm RIETAN-98 and its Applications to Zeolites. In: Delhez R, Mittemeijer EJ, editors. Materials Science Forum 321–324. Pfaffikon: Ttrans Tech Publications; 2000. pp. 198–205.

[31] Toraya H. Array-type universal profile function for powder pattern fitting. J. Appl. Crystallogr. 1990;23:485.

[32] Waasmaier D, Kirfel A. New analytical scattering-factor functions for free atoms and ions. Acta Cryst. 1995;A 51:416.

[33] Im M, Kweon SH, Kim JS, Nahm S, Choi JW, Hwang SJ. Microstructural variation and dielectric properties of KTiNbO$_5$ and K$_3$Ti$_5$NbO$_{14}$ ceramics. Ceram. Int. 2014;40:5861.

[34] Sugimoto W, Hirota N, Mimuro K, Sugahara Y, Kuroda K. Synthesis of reduced layered titanoniobates KTi$_{1-x}$Nb$_{1+x}$O$_5$. Mater. Lett. 1999;39:184.

[35] Navrotsky A, Muan A. Phase equilibria and thermodynamic properties of solid solutions in the systems ZnO·CoO·TiO$_2$ and ZnO·NiO·TiO$_2$ at 1050°C. J. Inorg. Nucl. Chem. 1970;32:3471.

[36] Glazer AM. Simple ways of determining perovskite structure. Acta Cryst. 1975;A 31:756.

[37] Kakimoto K, Shinkai Y. Structural characterization of Na$_{0.5}$K$_{0.5}$NbO$_3$ ceramic particles classified by centrifugal separator. Jpn. J. Appl. Phys.2011;Part 1 50:09NC13.

[38] Jia CL, Nagarajan V, He JQ, Houben L, Zhao T, Ramesh R, Urban K, Waser R. Unit-cell scale mapping of ferroelectricity and tetragonality in epitaxial ultrathin ferroelectric films. Nat. Mater. 2007;6:64.

[39] Uchino K, Nomura S. Critical exponents of the dielectric constants in diffused-phase-transition crystals. Ferroelectr. Lett. 1982;44:55.